CHAPTER 5

Bioconvective MHD Hybrid Nanofluid Flow past an Exponential Stretching Sheet *

5.1 INTRODUCTION

The stretching rate of sheets strongly affects the final product quality and, the exponential velocity and temperature distributions influence the admirable grade products attained in the annealing and thinning of copper wires.

This chapter analyses the magnetohydrodynamics of bioconvective hybrid nanofluid (TiO_2 and Ag in water) flow over a permeable exponential stretching sheet. The effects of thermal radiation, heat generation, chemical reaction, porosity, and viscous dissipation have been incorporated. Apposite similarity variables are applied in transforming the modeled PDE into an ODE system, and transmuted equations are solved numerically with the aid of the finite-difference-based bvp5c algorithm using MATLAB software. Multiple linear regression has been utilized to statistically scrutinize the effect of relevant variables on drag coefficient and heat transfer rate.

*Published in International Communications in Heat and Mass Transfer (Elsevier), 2022;135; 106115

5.2 MATHEMATICAL FORMULATION

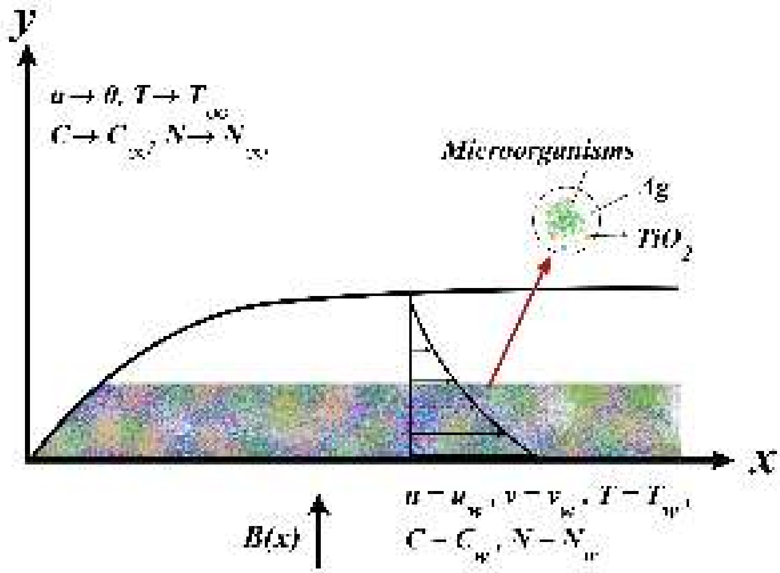

Figure 5.1: *Physical configuration*

Here a two-dimensional steady dissipative flow of hybrid nanofluid suspended with gyrotactic microorganisms through an exponentially stretching permeable sheet is contemplated. The x-axis is taken along the stretching surface and the y-axis is normal to the surface (illustrated in Figure 5.1). The sheet is stretched in x-direction ($x \geq 0$) with exponential velocity $u_w(x) = ce^{x/L}$. Velocity in y-direction is considered to be$v_w = v_0 e^{x/2L}$, since it is a permeable sheet. Here c and v_0 are positive constants and L is the reference length. The sheet is maintained at temperature $T_w = T_\infty + T_0 e^{x/2L}$, nanoparticle concentration $C_w = C_\infty + C_0 e^{x/2L}$, and microbial concentration $N_w = N_\infty + N_0 e^{x/2L}$ where T_0, C_0 and N_0 are constants, T_∞, C_∞, and N_∞ are corresponding, the ambient fluid temperature, nanoparticle concentration, and microbial concentration. The variable magnetic field $B(x) = B_0 e^{x/2L}$, where B_0 is uniform magnetic strength inflicted normally to the sheet. The consequence of the variable heat source $Q(x) = Q_0 e^{x/L}$, chemical reaction $K_l = K_0 e^{x/L}$, and porosity $K = K_r e^{-x/L}$ effects are also taken into account. Hence the governing equations see (Waini et al., 2020), (Pal & Mondal, (2018b), (Raju, Sandeep, Sugunamma, Babu, & Reddy, 2016) are:

$$\frac{\partial u}{\partial x} + \frac{\partial v}{\partial y} = 0 \tag{5.2.1}$$

$$u\frac{\partial u}{\partial x} + v\frac{\partial u}{\partial y} = \left(\frac{\mu_{hnf}}{\rho_{hnf}}\right)\frac{\partial^2 u}{\partial y^2} - \frac{\sigma_{hnf}}{\rho_{hnf}}B^2(x)\,u - \frac{\mu_{hnf}}{\rho_{hnf}}\frac{u}{K} \tag{5.2.2}$$

$$u\frac{\partial T}{\partial x} + v\frac{\partial T}{\partial y} = \alpha_{hnf}\frac{\partial^2 T}{\partial y^2} - \frac{1}{(\rho C_p)_{hnf}}\frac{\partial q_r}{\partial y} + \frac{Q}{(\rho C_p)_{hnf}}(T - T_\infty) + \frac{\mu_{hnf}}{(\rho C_p)_{hnf}}\left(\frac{\partial u}{\partial y}\right)^2 \tag{5.2.3}$$

$$u\frac{\partial C}{\partial x} + v\frac{\partial C}{\partial y} = D_B\frac{\partial^2 C}{\partial y^2} - K_l(C - C_\infty) \tag{5.2.4}$$

$$u\frac{\partial N}{\partial x} + v\frac{\partial N}{\partial y} + \frac{bW_c}{C_w - C_\infty}\left(\frac{\partial}{\partial y}\left(N\frac{\partial C}{\partial y}\right)\right) = D_m\frac{\partial^2 N}{\partial y^2} \tag{5.2.5}$$

subject to the boundary conditions:

$$\left.\begin{array}{c} u = u_w = ce^{x/L} \quad v = v_w = v_0 e^{x/2L} \quad T = T_w = T_\infty + T_0 e^{x/2L} \\ C = C_w = C_\infty + C_0 e^{x/2L}, \quad N = N_w = N_\infty + N_0 e^{x/2L} \end{array}\right\} \; at \; y = 0 \tag{5.2.6}$$

$$u \to 0, \quad T \to T_\infty, \quad C \to C_\infty, \quad N \to N_\infty \; as \; y \to \infty \tag{5.2.7}$$

The radiative heat flux q_r (in equation (5.2.3)) can be expressed as $q_r = -\frac{4\sigma^*}{3k^*}\frac{\partial T^4}{\partial y}$, where k^* and σ^* denote the mean absorption coefficient and Stefan-Boltzman constant, respectively. Using Taylor's series T^4 can be expressed as $T^4 \cong 4T_\infty^3 T - 3T_\infty^4$. Consider the following similarity variables (see (Waini et al., 2020) and (Shafiq et al., 2020)):

$$\begin{array}{lll} \eta = ye^{x/2L}\sqrt{c/2\vartheta_f L}, & u = ce^{x/L}f'(\eta), & v = -e^{\frac{x}{2L}}\sqrt{\frac{\vartheta_f c}{2L}}\left(f(\eta) + \eta f'(\eta)\right), \\ \theta(\eta) = \frac{T - T_\infty}{T_w - T_\infty}, & \psi(\eta) = \frac{C - C_\infty}{C_w - C_\infty}, & \chi(\eta) = \frac{N - N_\infty}{N_w - N_\infty} \end{array}$$

The effective thermophysical models of the hybrid nanofluid are given by:

Effective Dynamic Viscosity:

$$\frac{\mu_{hnf}}{\mu_f} = \frac{1}{(1-\phi_1)^{2.5}(1-\phi_2)^{2.5}} = \frac{1}{a_1}$$

Effective Density:

$$\frac{\rho_{hnf}}{\rho_f} = (1-\phi_2)\left[1-\phi_1+\phi_1\left(\frac{\rho_{s_1}}{\rho_f}\right)\right] + \ \phi_2\left(\frac{\rho_{s_2}}{\rho_f}\right) = a_2$$

Effective Electrical Conductivity:

$$\frac{\sigma_{hnf}}{\sigma_f} = 1 + \frac{3\left(\frac{\phi_1\sigma_1+\phi_2\sigma_2}{\sigma_f} - (\phi_1+\phi_2)\right)}{2+\left(\frac{\phi_1\sigma_1+\phi_2\sigma_2}{(\phi_1+\phi_2)\sigma_f}\right) - \left(\frac{\phi_1\sigma_1+\phi_2\sigma_2}{\sigma_f} - (\phi_1+\phi_2)\right)} = a_3$$

Effective Specific Heat:

$$\frac{(\rho C_p)_{hnf}}{(\rho C_p)_f} = (1-\phi_2)\left[1-\phi_1+\phi_1\left(\frac{(\rho c_p)_{s_1}}{(\rho c_p)_f}\right)\right] + \ \phi_2\left(\frac{(\rho c_p)_{s_2}}{(\rho c_p)_f}\right) = a_4$$

Effective Thermal Conductivity:

$$\frac{K_{hnf}}{K_f} = a_5$$

where

$$\frac{K_{hnf}}{K_{nf}} = \frac{K_{s_2}+2K_{nf}-2\phi_2\left(K_{nf}-K_{s_2}\right)}{K_{s_2}+2K_{nf}+2\phi_2\left(K_{nf}-K_{s_2}\right)}$$

and

$$\frac{K_{nf}}{K_f} = \frac{K_{s_1}+2K_f-2\phi_1\left(K_f-K_{s_1}\right)}{K_{s_1}+2K_f+\phi_1\left(K_f-K_{s_1}\right)}$$

In view of the above-mentioned similarity variables and effective thermophysical model, one can get the following from equations (5.2.1) – (5.2.7):

$$f''' + a_1a_2ff'' - f'\left(a_1a_3H + K_p + 2a_1a_2f'\right) = 0 \tag{5.2.8}$$

$$a_1\left(a_5+\frac{4}{3}R\right)\theta'' + a_1a_4Prf\theta' + a_1\,\mathrm{Pr}\left(\beta - a_4f'\right)\theta + PrEcf''^2 = 0 \tag{5.2.9}$$

$$\psi'' + Lef\psi' - Le\left(f'+K_c\right)\psi = 0 \tag{5.2.10}$$

$$\chi'' - Lb\left(f'\chi - f\chi'\right) - Pe\left\{(\chi+\Omega)\,\psi'' + \psi'\chi'\right\} = 0 \tag{5.2.11}$$

with

$$f(0) = S,\quad f'(0) = 1,\quad \theta(0) = 1,\quad \psi(0) = 1,\quad \chi(0) = 1 \tag{5.2.12}$$

$$f'(\infty)\to 0,\quad \theta(\infty)\to 0\quad \psi(\infty)\to 0\quad \chi(\infty)\to 0 \tag{5.2.13}$$

5.3 PHYSICAL QUANTITIES

The drag coefficients, local Nusselt number, local Sherwood number, and local microorganisms density number are given by (see (Waini et al., 2020) and (Pal & Mondal, (2018b)):

$$Cf_x = \frac{\tau_w}{\rho_f (u_w)^2} = \frac{\mu_{hnf}\left(\frac{\partial u}{\partial y}\right)_{y=0}}{\rho_f (u_w)^2} \Rightarrow Re_x^{1/2} Cf_x = \frac{f''(0)}{a_1}. \quad (5.3.1)$$

$$Nu_x = \frac{2Lq_w}{K_f (T_w - T_\infty)} = \frac{2L\left(-K_{hnf}\left(\frac{\partial T}{\partial y}\right)_{y=0} + (q_r)_{y=0}\right)}{K_f (T_w - T_\infty)} \Rightarrow$$
$$Re_x^{-1/2} Nu_x = -\left(a_5 + \frac{4}{3}R\right)\theta'(0) \quad (5.3.2)$$

$$Sh_x = \frac{2Lq_m}{D_B (C_w - C_\infty)} = -\frac{2LD_B\left(\frac{\partial C}{\partial y}\right)_{y=0}}{D_B (C_w - C_\infty)} \Rightarrow Re_x^{-1/2} Sh_x = -\psi'(0) \quad (5.3.3)$$

$$Nn_x = \frac{2Lq_n}{D_m (N_w - N_\infty)} = -\frac{2LD_m\left(\frac{\partial N}{\partial y}\right)_{y=0}}{D_m (N_w - N_\infty)} \Rightarrow Re_x^{-1/2} Nn_x = -\chi'(0) \quad (5.3.4)$$

where $Re_x = \frac{2Lu_w}{\vartheta_f}$ is the local Reynold's number.

5.4 NUMERICAL PROCEDURE

The transmuted Eqs. (5.2.8) – (5.2.13) are reduced into a system of single-order ordinary differential equations (ODEs) by setting:

$f = y_1.\quad f' = y_2,\quad f'' = y_3,\quad \theta = y_4,\quad \theta' = y_5,$

$\psi = y_6,\quad \psi' = y_7,\quad \chi = y_8,\quad \chi' = y_9$

The subsequent system of single-order ODEs is given by:

$$y_1' = y_2,\quad y_2' = y_3,\quad y_3' = y_2\left(a_1 a_3 H + K_p + 2a_1 a_2 y_2\right) - a_1 a_2 y_1 y_3,$$

$$y_4' = y_5,\quad y_5' = -\frac{\left(a_1 a_4 Pr y_1 y_5 + a_1 \Pr(\beta - a_4 y_2) y_4 + \Pr Ec\ y_3^2\right)}{a_1\left(a_5 + \frac{4}{3}R\right)},$$

$$y_6' = y_7,\quad y_7' = Le\left((y_2 + K_c) y_6 - y_1 y_7\right),$$

$$y_8' = y_9,\quad y_9' = Lb\left(y_2 y_8 - y_1 y_9\right) + Pe\left\{(y_8 + \Omega) y_7' + y_7 y_9\right\}$$

with

$$y_1(0) = S,\ y_2(0) = 1,\ y_4(0) = 1,\ y_6(0) = 1,\ y_8(0) = 1,$$

$$y_2(\infty) = 0,\ y_4(\infty) = 0,\ y_6(\infty) = 0,\ y_8(\infty) = 0.$$

The above system has been solved numerically using the finite-difference based bvp5c algorithm with infinity fixed at 5. The reliability of the adopted numerical method has been validated through a restrictive correspondence of the surface temperature gradient ($-\theta'(0)$) with the previously published works (Waini et al., 2020), (Magyari & Keller, 1999a) and (Abd El-Aziz, 2009) and a commendable agreement is observed (see Table 5.1).

5.5 RESULTS AND DISCUSSION

The impact of pertinent parameters on velocity ($f'(\eta)$), temperature ($\theta(\eta)$), nanoparticle concentration ($\psi(\eta)$), and microbial concentration ($\chi(\eta)$) profiles are illustrated through Figures 5.2 – 5.21. The thermophysical values of base fluid (water) and nanoparticles (TiO_2 and Ag) are displayed in Table 5.2. The Prandtl number (Pr) is set to 6.2 and $0.5 \leq H, R, K_p \leq 3, 0.1 \leq S, Ec, Pe \leq 0.6, 0 \leq \beta \leq 0.25, 0.3 \leq K_c, \Omega \leq 0.8, 1.2 \leq Le \leq 2.2, 0.6 \leq Lb \leq 1.6, 0 \leq \phi_1, \phi_2 \leq 0.1$ represent the considered range of the effectual parameters.

The Lorentz force generated due to an enhancement in the magnetic field parameter (H) resists the fluid flow that reduces the fluid velocity (displayed in Figure 5.2). Figure 5.3 illustrates the negative impact of the porosity parameter (K_p) on the velocity profile. This is physically attributed to the fact that an increase in K_p drops the magnitude of Darcian body force and hence slows the fluid. Figure 5.4 describes the changes in the suction parameter (S) is inversely proportional to $f'(\eta)$. This is in accordance with the physical fact with increasing values of S, the momentum boundary layer tends to stick with the stretching sheet that disturbs the flow momentum.

Figure 5.5 indicates the enhancement in $\theta(\eta)$ with H. This is because the generated Lorentz force (due to the changes in H) increases the friction between the fluid layers that enhance the temperature profile. The upshot of radiation parameter (R) on $\theta(\eta)$ is exhibited in Figure 5.6. Greater values of R produce greater surface heat flux that improves the fluid temperature. Figure 5.7 depicts the positive impact of Eckert number (Ec) on $\theta(\eta)$. The elevation in the temperature profile is physically associated with the production of frictional energy caused by the collision of fluid particles. The heat source (β) and porosity (K_p) parameters generate an internal heat (see (Mandal & Mukhopadhyay, 2013) and (Naramgari & Sulochana, 2016)) that elevates the temperature profile (see Figures 5.8 and 5.9, respectively). Figure 5.10 elucidate the consequence of S on $\theta(\eta)$. Augmentation in S increases the fluid's absorption rate (towards the surface) and hence reduces the fluid temperature. The positive influence of volume fraction of TiO_2 and Ag nanoparticles on $\theta(\eta)$ is depicted in Figures 5.11 and 5.12, respectively. Physically, this is due to the increased particle collision and improved thermal conductivity of the fluid caused by the addition of TiO_2 and Ag nanoparticles.

The Lorentz force generated with the magnification of H induces a disturbance in the fluid motion that enlarges the solutal boundary layer thickness (see Figure 5.13). An increase in the chemical reaction parameter (K_c) expedites the nanoparticle consumption causing a drop in $\psi(\eta)$ (shown in Figure 5.14). The negative response of S on $\psi(\eta)$ has been graphed in Figure 5.15. This decrease in $\psi(\eta)$ is physically attributed to the fact that an improvement in S brings the fluid closer to the surface that reduces the solutal boundary layer thickness. An increase in Lewis number (Le) reduces the mass diffusivity thereby causing a decline in the concentration profile (see Figure 5.16).

Figures 5.17 and 5.18 elucidate the positive impact of H and K_p on $\chi(\eta)$, respectively. The disturbance in the fluid motion caused by the changes in H and K_p generates heat that boosts the microorganism boundary layer thickness. Figure 5.19 graphs the decreasing nature of $\chi(\eta)$ with respect to Peclet number (Pe). Physically, augmentation in Pe intensifies the microbial movement that reduces the microorgaism density near the surface. The diffusivity of the microorganisms descends with mounting values of bioconvection Lewis number (Lb) that reduces the microorganism density of the fluid (shown in Figure 5.20). Figure 5.21 bespeaks the deviations in $\chi(\eta)$ with respect to microbial concentration difference parameter (Ω). Physically, this decrease in $\chi(\eta)$ is due to the fact that higher values of Ω implies larger density difference between the gyrotactic microorganisms and base fluid that makes the surface of the fluid unstable forcing the microorganisms to swim back to the fluid's bottom layer.

The simultaneous influence of influential parameters on the mass transfer rate has been displayed in Figures 5.22 and 5.23 with the aid of three-dimensional surface plots. It is observed that the mass transfer rate is a decreasing function of K_p and an increasing function of S. Higher values of K_c consume more nanoparticles thereby lowering the concentration of the fluid that enhances the mass transfer rate (see Figure 5.22). Furthermore, enhanced kinetic energy due to the addition of TiO_2 nanoparticles increase the mass transfer rate (See Figure 5.23).

The consequence of prominent parameters on drag coefficient, Nusselt number, and microorganism density number have been carried out in Tables 5.3 – 5.5. The slope of linear regression has also been calculated. The magnitude of slope represents the rate of change of the considered physical quantity per unit value of the corresponding parameter and the sign of slope symbolizes the nature of this impact. The drag coefficient declines with changes in H, K_p, S, ϕ_1, and ϕ_2 values (see Table 5.3). The restricted flow due to these variables reduces the drag coefficient. The rate of heat transfer ascends with R (since R improves surface heat flux) but descends with an increase in H, Ec, β, ϕ_1, and ϕ_2 values (see Table 5.4). The internal heat generated due to these variables reduces the temperature difference between the surface and the fluid which lowers the heat transfer rate. The microorganism density number descends with K_p and ascends with K_c, Pe, Ω, Le, and Lb (see Table 5.5). Augmentation in K_p values reduce the fluid motion that demotes the microorganism density number. A rise in the chemical reaction parameter consumes more nanoparticles and decreases the concentration of the chemical species. This causes a decrease in the fluid's density that promotes the movement of more microorganisms to the vacant area and thereby increases the microorganism density number.

5.6 STATISTICAL ANALYSIS

The use of statistical techniques like probable error, correlation, and multiple linear regression to scrutinize the numerical and estimated results have gained a lot of interest from the research community. In this study, the effect of pertinent parameters on drag coefficient and heat transfer rate have been statistically scrutinized.

5.6.1 Correlation and probable error

Correlation measures the degree of association between two or more variables. The magnitude of the correlation coefficient (r), where $r \in [-1, 1]$, indicates the strength of the relationship and the sign of r represents the nature of this relationship. The integrity of r is further clarified using probable error, $PE = (\frac{1-r^2}{\sqrt{n}})0.6745$ where n is the number of observations. If $\left|\frac{r}{PE}\right| > 6$, then the correlation is said to be significant.

From Table 5.6, it is noted that $Cf_x {Re_x}^{1/2}$ is negatively correlated with H, K_p, S, ϕ_1 and ϕ_2. $Nu_x {Re_x}^{-1/2}$ is positively correlated with R and negatively correlated with H, Ec, β, ϕ_1, and ϕ_2 (see Table 5.7). Furthermore, it is observed that these findings coincide with the results obtained in Tables 5.3 and 5.4.

5.6.2 Multiple linear regression

Regression analysis judges the relationship between responses (dependent variable) and one or more predictors (independent variables). All correlations are found to be significant and hence $Cf_x {Re_x}^{1/2}$ and $Nu_x {Re_x}^{-1/2}$are estimated using multiple regression analysis. The general forms of the estimated models are given by:

$$Cf_{est} = b_H H + b_{K_p} K_p + b_S S + b_{\phi_1}\phi_1 + b_{\phi_2}\phi_2 + b_0$$

$$Nu_{est} = b_H H + b_{Ec} Ec + b_R R + b_\beta \beta + b_{\phi_1}\phi_1 + b_{\phi_2}\phi_2 + b_0$$

where $b_H, b_{K_p}, b_S, b_{Ec}, b_R, b_\beta, b_{\phi_1}, b_{\phi_2}, b_\theta$ are the estimated regression coefficients.

The drag coefficient is estimated from 30 sets of values chosen in the range [0.5,3] for H and K_p, [0.01,0.1] for ϕ_1 and ϕ_2, and [0.1,0.6] for S. Further, the heat transfer rate is evaluated from 36 sets of values chosen in the range [0.5,3] for H and R, [0.01,0.1] for ϕ_1 and ϕ_2,[0.1,0.6] for Ec, and [0.05,0.3] for β. The regression coefficients (for both cases) are found using Microsoft Excel. The estimated regression models are given by:

$$Cf_{est} = -0.39712\ H - 0.38537\ K_p - 1.21825\ S - 7.4983\ \phi_1 - 10.3397\ \phi_2 - 0.89767$$

$$\begin{aligned} Nu_{est} = -0.61526\ H - 9.26793\ Ec + 0.189206\ R - 9.16537\ \beta - 5.50554\ \phi_1 \\ - 9.71937\ \phi_2 + 6.557836 \end{aligned}$$

The positive sign of the estimated regression coefficient denotes that the corresponding parameter ascends the drag coefficient or the heat transfer rate and a negative sign of the estimated regression coefficient denotes that the corresponding parameter descends the drag coefficient or the heat transfer rate. From the estimated models, it can be observed that the drag coefficient declines with increasing values of H, K_p, S, ϕ_1, and ϕ_2. Furthermore, it is also noted that the heat transfer rate enhances with augmentation in R and reduces with increasing values of H, Ec, β, ϕ_1, and ϕ_2. These results are in perfect agreement with the findings in Tables 5.3, 5.4, 5.6 and 5.7. The accuracy of the estimated regression model (for the chosen sample) has been adjudged through Figures. 5.24 and 5.25. A commendable agreement is noted between the actual and estimated values.

5.7 CONCLUSION

For its application in metal spinning, drawing of plastic films, glass blowing, crystal growing, and cooling of filaments; the dynamics of bioconvective MHD hybrid nanofluid (TiO_2 and Ag in water) flow over a permeable exponential stretching surface in the presence of thermal radiation, heat generation, chemical reaction, porosity, and dissipative effects has been investigated. The consequence of effectual variables on the flow profiles has been numerically solved with the aid of the finite-difference-based bvp5c algorithm. Further, multiple linear regression has been utilized to statistically scrutinize the effect of pertinent parameters on drag coefficient and heat transfer rate. The major conclusions drawn from the study are:

- The magnetic field has a destructive effect on the velocity profile and a constructive effect on the temperature, nanoparticle concentration, and microbial concentration profiles.
- An increase in the porosity parameter descends the velocity profile and ascends the temperature and microbial concentration profiles.
- The temperature profile is proportional to augmentations in radiation parameter, magnetic field parameter, Eckert number, and volume fraction of TiO_2 and Ag nanoparticles.
- Nanoparticle concentration is a decreasing function of Lewis number and chemical reaction parameter.
- The mass transfer rate is inversely proportional to the changes in the porosity

parameter and directly proportional to the changes in the chemical reaction and suction parameters.

- The local microbial density number declines with growing values of porosity parameter and improves with growing values of the chemical reaction parameter and Peclet number.

- The estimated regression model for the drag coefficient is given by:

$$Cf_{est} = -0.39712\,H - 0.38537\,K_p - 1.21825\,S - 7.4983\,\phi_1 - 10.3397\,\phi_2 - 0.89767$$

- The estimated regression model for the heat transfer rate is given by:

$$Nu_{est} = -0.61526\ H - 9.26793\ Ec + 0.189206\ R - 9.16537\ \beta - 5.50554\ \phi_1 - 9.71937\ \phi_2 + 6.557836$$

- The drag coefficient is negatively correlated with the magnetic parameter, suction parameter, porosity parameter, and volume fraction of TiO_2 and Ag nanoparticles.

- The heat transfer rate is positively correlated with the radiation parameter and negatively correlated with the magnetic parameter, heat source parameter, viscous dissipation parameter, and volume fraction of TiO_2 and Ag nanoparticles.

TABLES AND GRAPHS

Table 5.1: *Comparison of $-\theta'(0)$ for different values of Pr when $\phi_1 = \phi_2 = M = R = Ec = Le = Lb = K_c = K_p = \beta = \Omega = Pe = S = 0$*

Pr	(Magyari & Keller, 1999a)	(Abd El-Aziz, 2009)	(Waini et al., 2020)	**Present Study**
0.5	0.5943	0.5945	0.5943	0.5945
1	0.9548	0.9548	0.9548	0.9548
3	1.8691	1.8691	1.8691	1.8691
5	2.5001	2.5001	2.5001	2.5001
10	3.6604	3.6604	3.6604	3.6604

Table 5.2: *Thermophysical properties*

Properties	H_2O	TiO_2	Ag
ρ	997.1	4250	10500
C_p	4179	686.2	235
k	0.613	8.9538	429
σ	$5 * 10^{-2}$	$2.38 * 10^6$	$3.5 * 10^6$

Table 5.3: *Variation in* $Cf_xRe_x^{1/2}$ *when* $Pr = 6.2, R = 1, Ec = 0.3, Le = 2, K_c = \Omega = Pe = 0.5, \beta = 0.1,$ *and* $Lb = 1.2$

H	K_p	S	ϕ_1	ϕ_2	$Cf_xRe_x^{1/2}$
0.5	1	0.1	0.1	0.1	-3.3727
1	1	0.1	0.1	0.1	-3.5937
1.5	1	0.1	0.1	0.1	-3.8012
2	1	0.1	0.1	0.1	-3.9975
Slope					**-0.4166**
1	0.5	0.1	0.1	0.1	-3.38
1	1	0.1	0.1	0.1	-3.5937
1	1.5	0.1	0.1	0.1	-3.7947
1	2	0.1	0.1	0.1	-3.9852
Slope					**-0.4034**
1	1	0.1	0.1	0.1	-3.5937
1	1	0.2	0.1	0.1	-3.7076
1	1	0.3	0.1	0.1	-3.8253
1	1	0.4	0.1	0.1	-3.9466
Slope					**-1.1765**
1	1	0.1	0.01	0.1	-2.924
1	1	0.1	0.02	0.1	-2.9904
1	1	0.1	0.03	0.1	-3.0586
1	1	0.1	0.04	0.1	-3.1287
Slope					**-6.8242**
1	1	0.1	0.1	0.01	-2.6673
1	1	0.1	0.1	0.02	-2.7629
1	1	0.1	0.1	0.03	-2.86
1	1	0.1	0.1	0.04	-2.9588
Slope					**-9.7153**

Table 5.4: *Variation in* $Cf_xRe_x^{1/2}$ *when* $Pr = 6.2, R = 1, Ec = 0.3, Le = 2, K_c = \Omega = Pe = 0.5, \beta = 0.1,$ *and* $Lb = 1.2$

H	K_p	S	ϕ_1	ϕ_2	$Cf_xRe_x^{1/2}$
0.5	1	0.1	0.1	0.1	-3.3727
1	1	0.1	0.1	0.1	-3.5937
1.5	1	0.1	0.1	0.1	-3.8012
2	1	0.1	0.1	0.1	-3.9975
Slope					**-0.4166**
1	0.5	0.1	0.1	0.1	-3.38
1	1	0.1	0.1	0.1	-3.5937
1	1.5	0.1	0.1	0.1	-3.7947
1	2	0.1	0.1	0.1	-3.9852
Slope					**-0.4034**
1	1	0.1	0.1	0.1	-3.5937
1	1	0.2	0.1	0.1	-3.7076
1	1	0.3	0.1	0.1	-3.8253
1	1	0.4	0.1	0.1	-3.9466
Slope					**-1.1765**
1	1	0.1	0.01	0.1	-2.924
1	1	0.1	0.02	0.1	-2.9904
1	1	0.1	0.03	0.1	-3.0586
1	1	0.1	0.04	0.1	-3.1287
Slope					**-6.8242**
1	1	0.1	0.1	0.01	-2.6673
1	1	0.1	0.1	0.02	-2.7629
1	1	0.1	0.1	0.03	-2.86
1	1	0.1	0.1	0.04	-2.9588
Slope					**-9.7153**

Table 5.5: *Variation in $Nu_xRe_x^{-1/2}$ when $Pr = 6.2, Le = 2, K_c = \Omega = Pe = 0.5, K_p = 1, Lb = 1.2$ and $S = 0.1$*

H	Ec	R	β	ϕ_1	ϕ_2	$Nu_xRe_x^{-1/2}$
0.5	0.3	1	0.1	0.1	0.1	1.25895
1	0.3	1	0.1	0.1	0.1	0.90999
1.5	0.3	1	0.1	0.1	0.1	0.58361
Slope						**-0.6753**
1	0.1	1	0.1	0.1	0.1	2.76283
1	0.2	1	0.1	0.1	0.1	1.83641
1	0.3	1	0.1	0.1	0.1	0.90999
Slope						**-9.2642**
1	0.3	0.5	0.1	0.1	0.1	0.78785
1	0.3	1	0.1	0.1	0.1	0.90999
1	0.3	1.5	0.1	0.1	0.1	1.00861
Slope						**0.22075**
1	0.3	1	0.15	0.1	0.1	0.61246
1	0.3	1	0.2	0.1	0.1	0.23675
1	0.3	1	0.25	0.1	0.1	-0.2966
Slope						**-9.0907**
1	0.3	1	0.1	0.01	0.1	1.39817
1	0.3	1	0.1	0.02	0.1	1.34932
1	0.3	1	0.1	0.03	0.1	1.29927
Slope						**-4.945**
1	0.3	1	0.1	0.1	0.01	1.78003
1	0.3	1	0.1	0.1	0.02	1.68727
1	0.3	1	0.1	0.1	0.03	1.59375
Slope						**-9.3141**

Table 5.6: *Variation in $Nn_xRe_x^{-1/2}$ when $Pr = 6.2, H = R = 1, S = \beta = \phi_1 = \phi_2 = 0.1,$ and $Ec = 0.3$*

K_p	K_c	Pe	Ω	Le	Lb	$Nn_xRe_x^{-1/2}$
0.5	0.5	0.5	0.5	2	1.2	2.13076
1	0.5	0.5	0.5	2	1.2	2.1024
1.5	0.5	0.5	0.5	2	1.2	2.07662
Slope						**-0.0542**
1	0.4	0.5	0.5	2	1.2	2.0549
1	0.5	0.5	0.5	2	1.2	2.1024
1	0.6	0.5	0.5	2	1.2	2.14748
Slope						**0.46289**
1	0.5	0.4	0.5	2	1.2	1.87087
1	0.5	0.5	0.5	2	1.2	2.1024
1	0.5	0.6	0.5	2	1.2	2.33564
Slope						**2.32388**
1	0.5	0.5	0.4	2	1.2	2.02874
1	0.5	0.5	0.5	2	1.2	2.1024
1	0.5	0.5	0.6	2	1.2	2.17607
Slope						**0.73665**
1	0.5	0.5	0.5	1.8	1.2	2.02589
1	0.5	0.5	0.5	2	1.2	2.1024
1	0.5	0.5	0.5	2.2	1.2	2.17615
Slope						**0.37565**
1	0.5	0.5	0.5	2	1	2.00053
1	0.5	0.5	0.5	2	1.2	2.1024
1	0.5	0.5	0.5	2	1.4	2.20067
Slope						**0.50036**

Table 5.7: *Correlation coefficient (r), probable error (PE), and $\left|\frac{r}{PE}\right|$ values of $Cf_xRe_x^{1/2}$*

Parameter	r	PE	$\left\|\frac{r}{PE}\right\|$
H	-0.9992	0.00042	2357.25
K_p	-0.9993	0.0004	2521.01
S	-0.9998	0.00014	7262.22
ϕ_1	-0.9998	0.00011	9078
ϕ_2	-0.9999	4.41E-05	22696.4

Table 5.8: *Correlation coefficient* (r), *probable error* (PE), *and* $\left|\frac{r}{PE}\right|$ *values of* $Nu_x Re_x^{-1/2}$

Parameter	r	PE	$\left\|\frac{r}{PE}\right\|$
H	-0.9991	0.00051	1972.77
Ec	-1	0	#DIV/0!
R	0.99864	0.00075	1332.26
β	-0.9657	0.01858	51.9837
ϕ_1	-0.9998	9.36E-05	10680.2
ϕ_2	-1	1.10E-05	90788.2

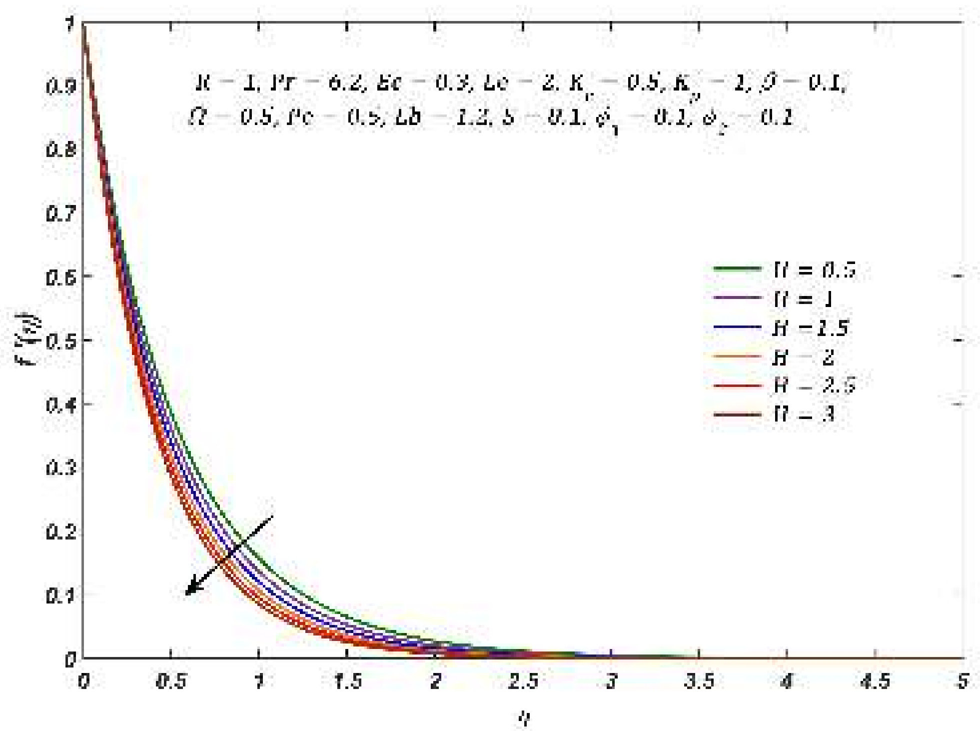

Figure 5.2: *Variation in* $f'(\eta)$ *with* M

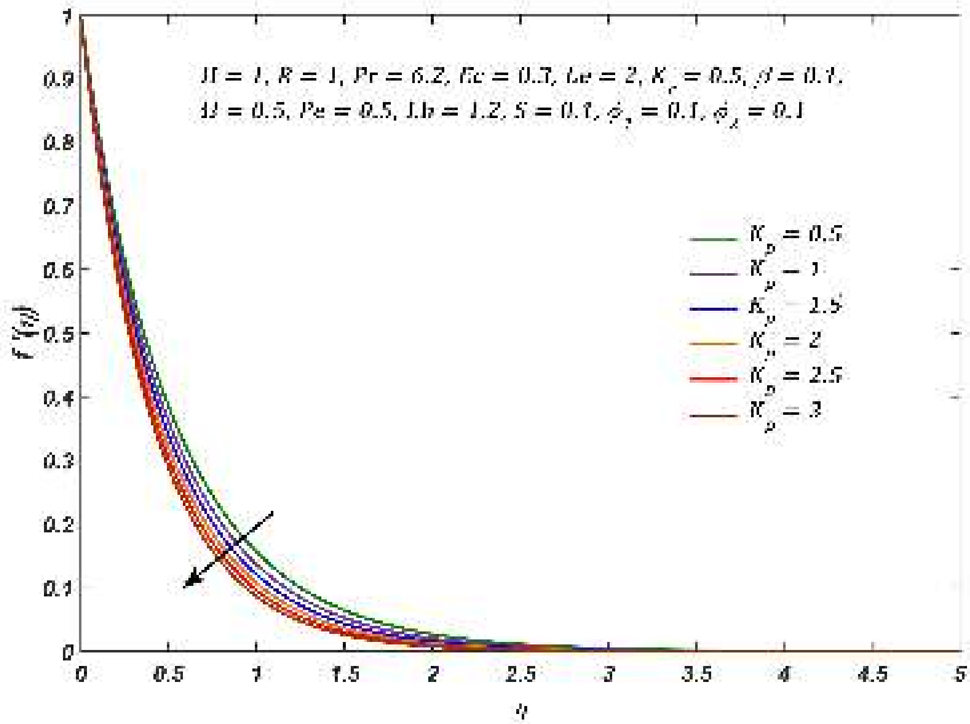

Figure 5.3: *Variation in $f'(\eta)$ with K_p*

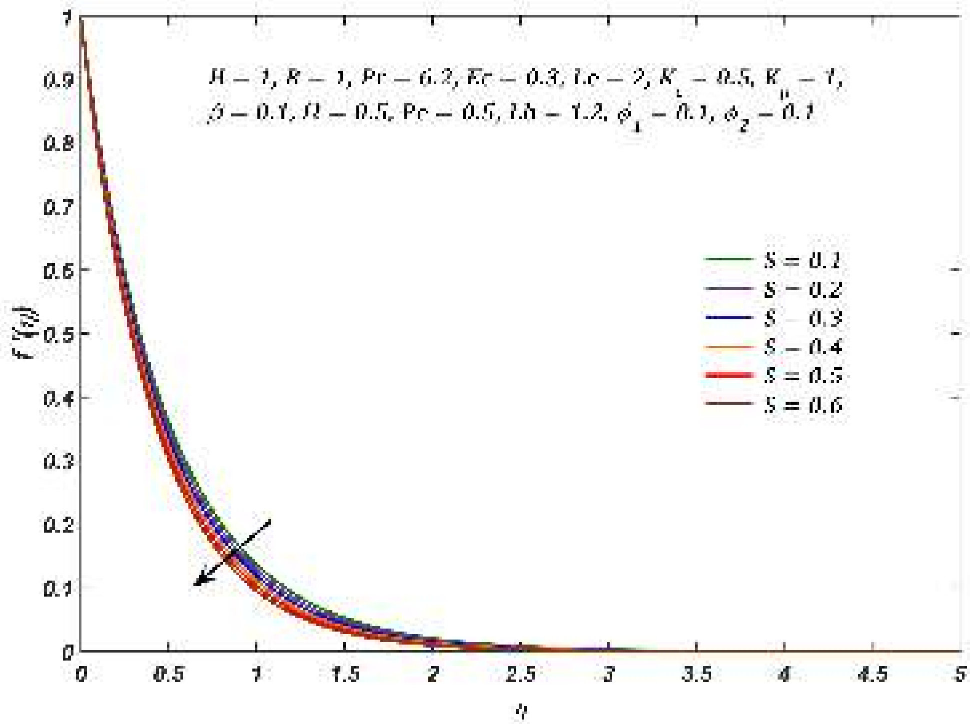

Figure 5.4: *Variation in $f'(\eta)$ with S*

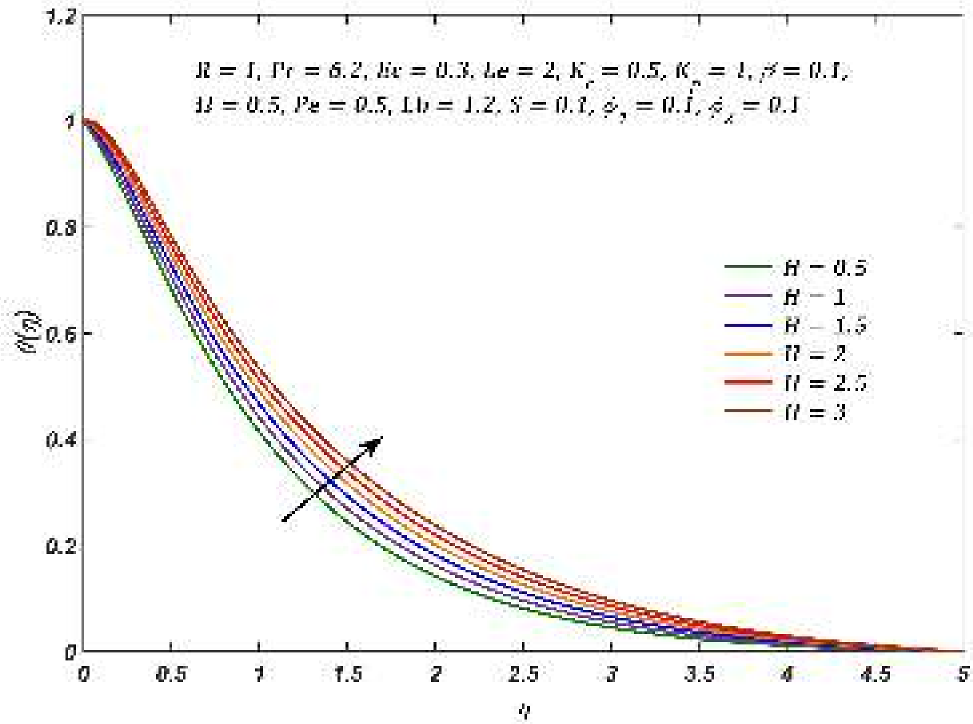

Figure 5.5: *Variation in $\theta(\eta)$ with M*

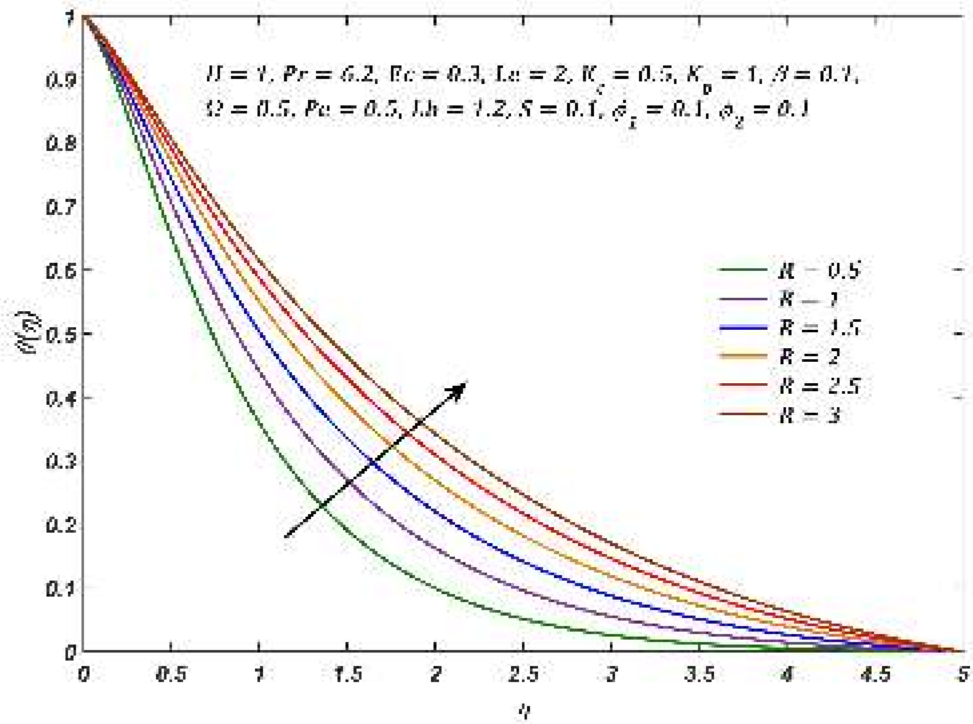

Figure 5.6: *Variation in $\theta(\eta)$ with R*

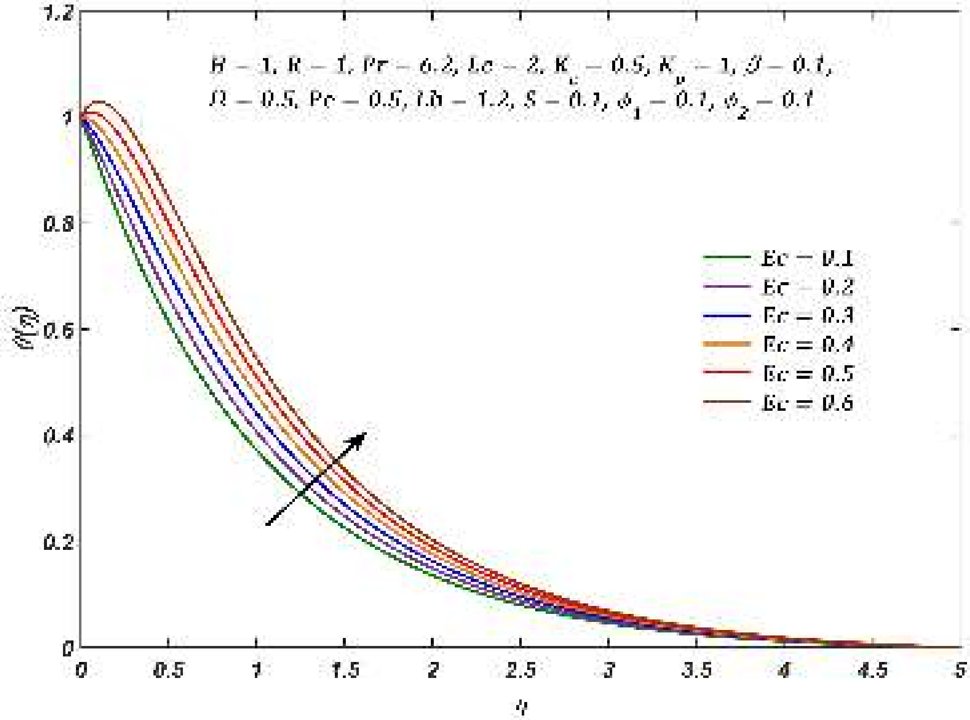

Figure 5.7: *Variation in $\theta(\eta)$ with Ec*

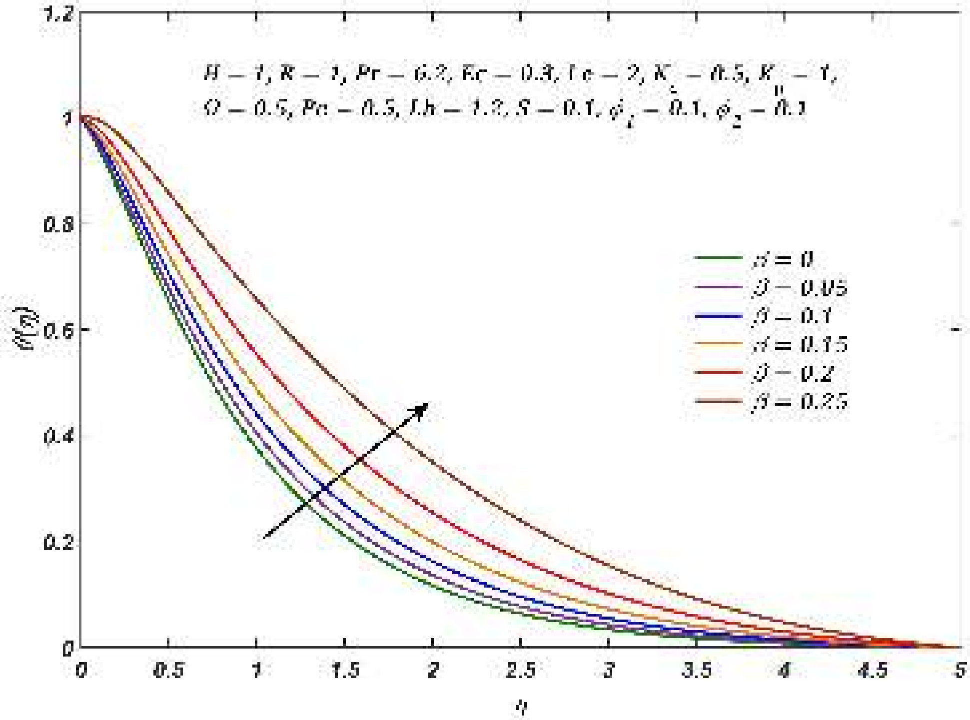

Figure 5.8: *Variation in $\theta(\eta)$ with β*

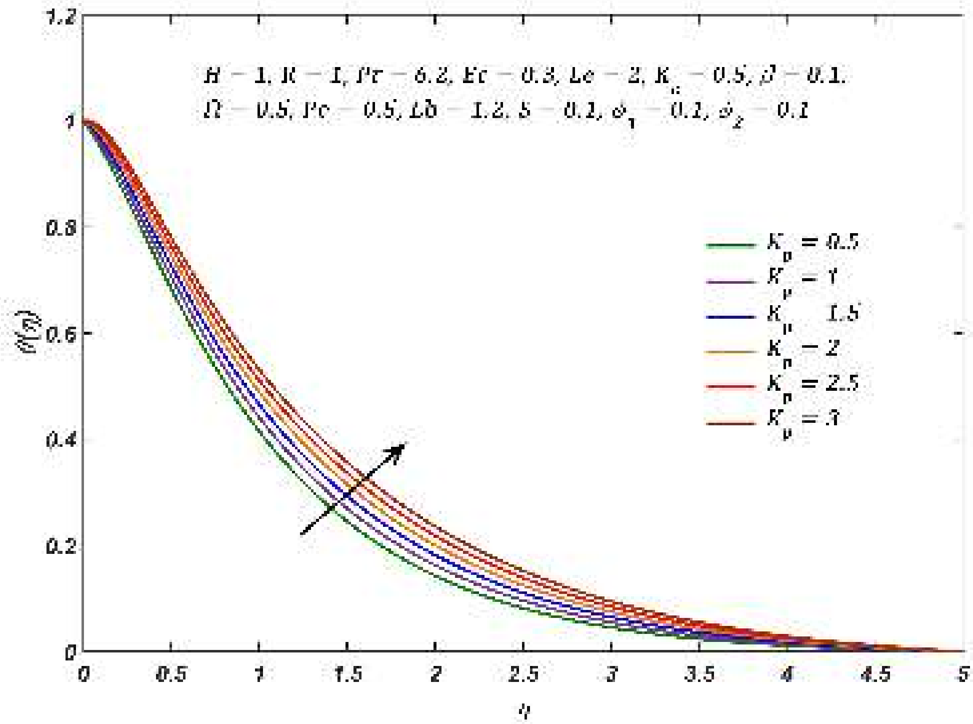

Figure 5.9: *Variation in* $\theta(\eta)$ *with* K_p

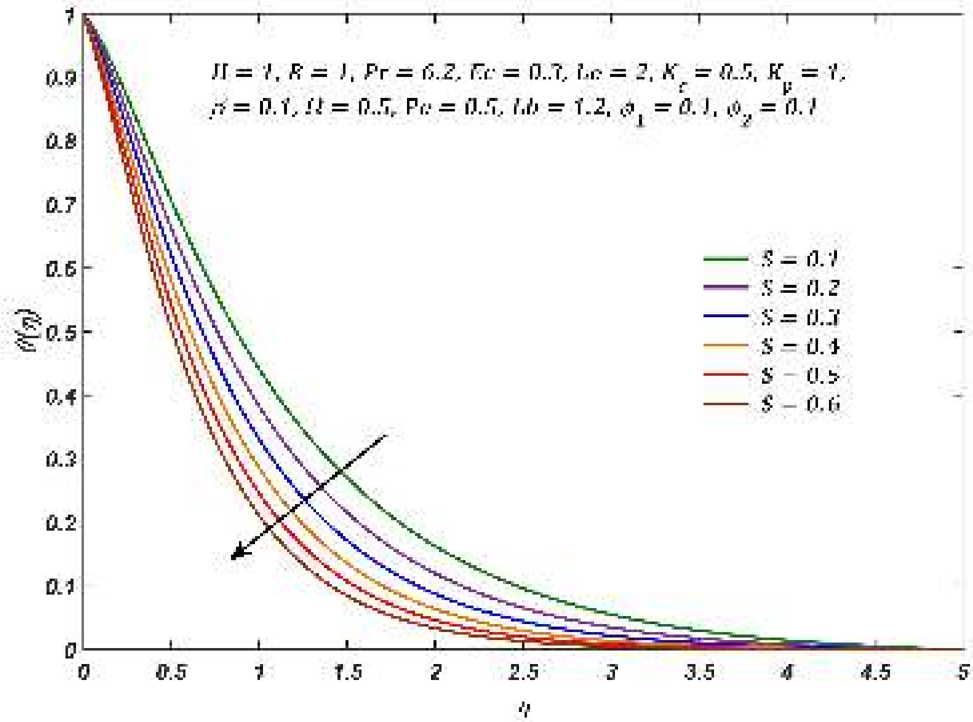

Figure 5.10: *Variation in* $\theta(\eta)$ *with* S

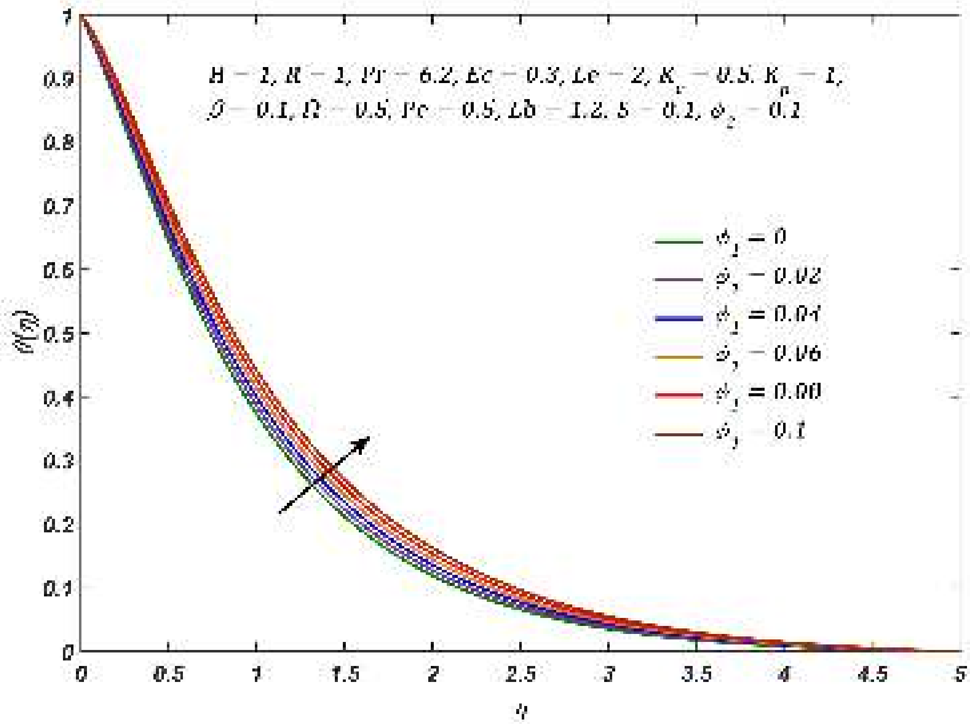

Figure 5.11: *Variation in* $\theta(\eta)$ *with* ϕ_1

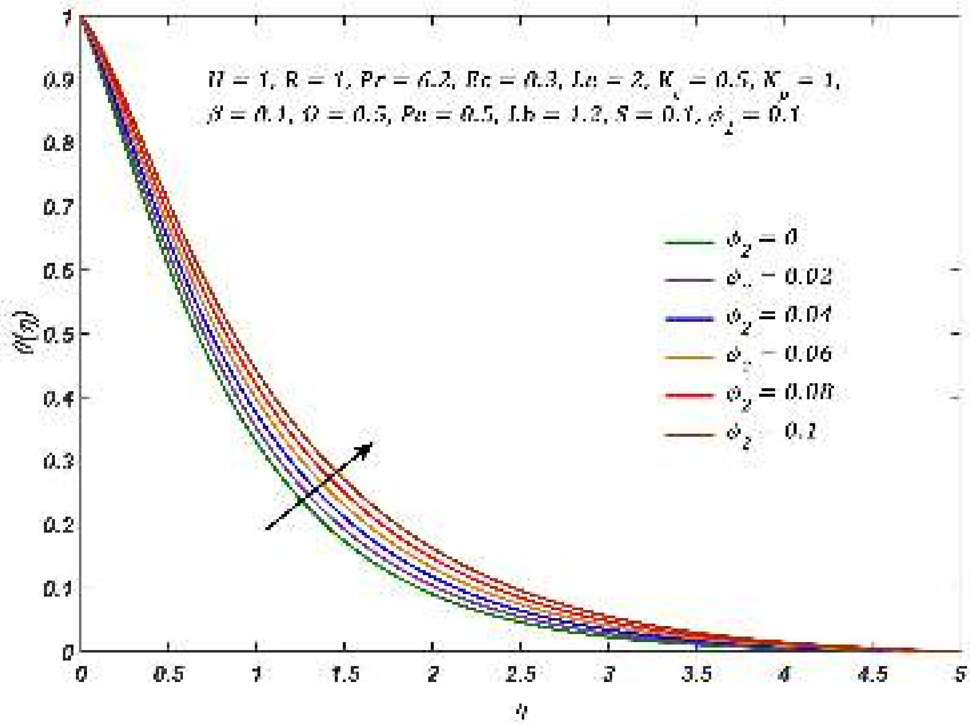

Figure 5.12: *Variation in* $\theta(\eta)$ *with* ϕ_2

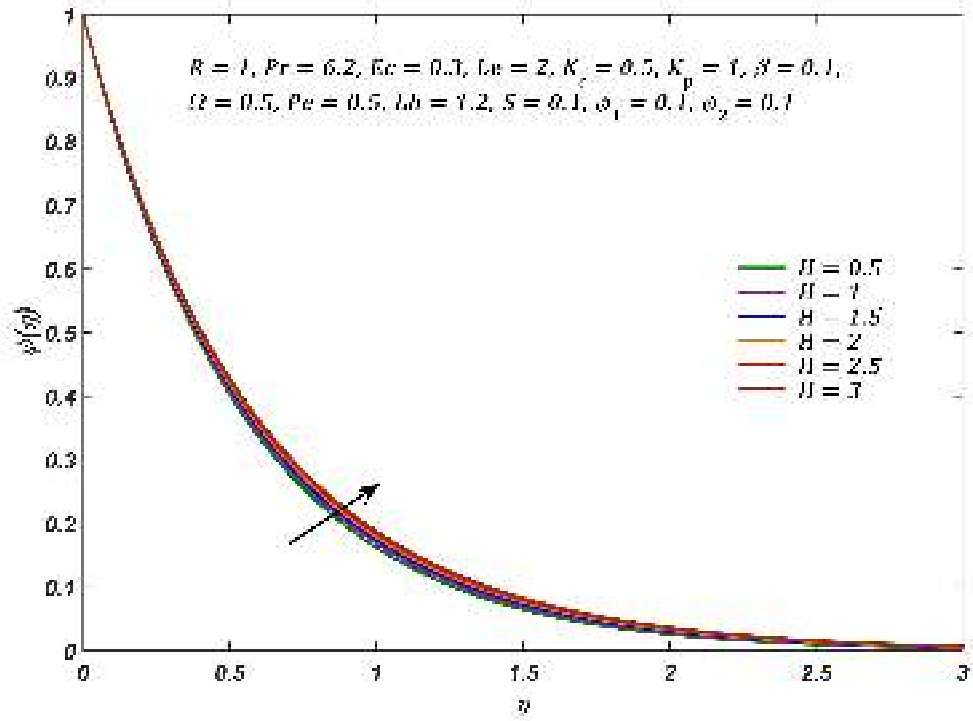

Figure 5.13: *Variation in* $\psi(\eta)$ *with* M

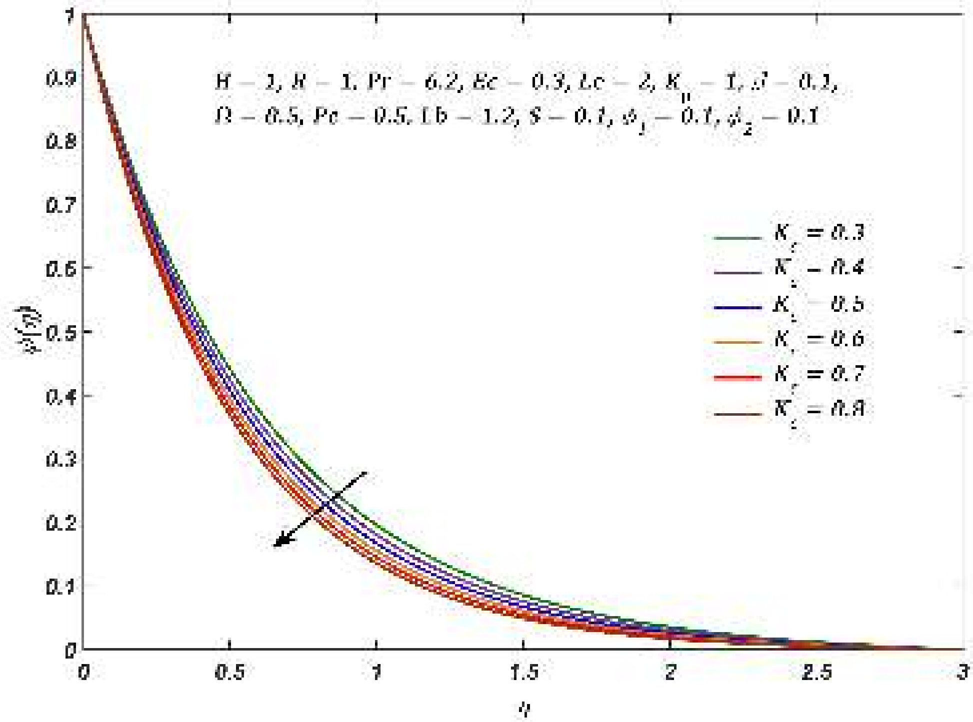

Figure 5.14: *Variation in* $\psi(\eta)$ *with* K_c

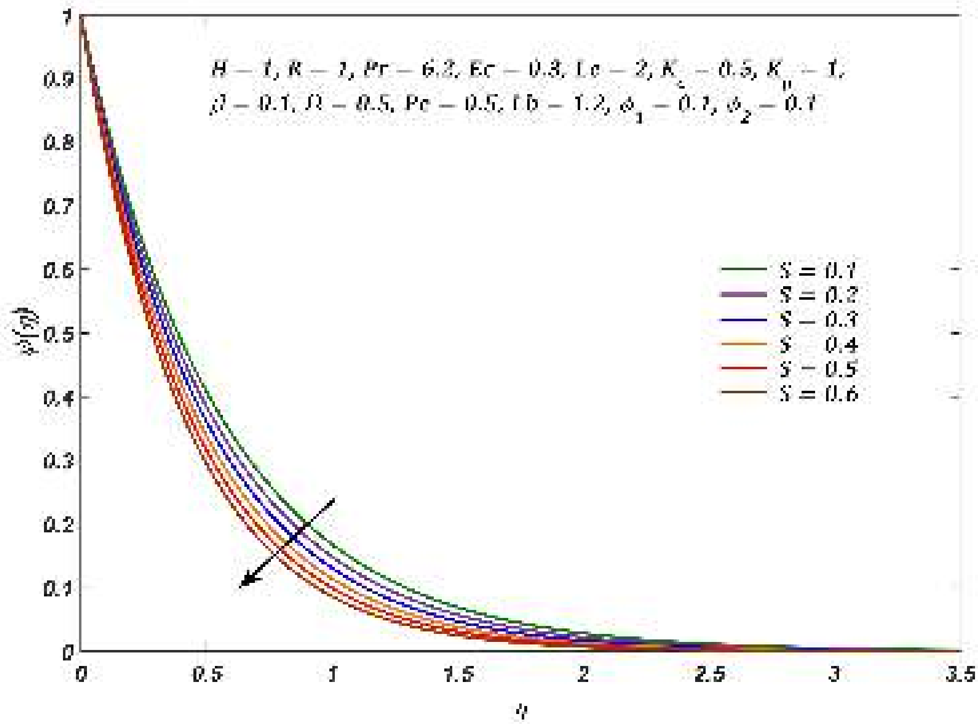

Figure 5.15: *Variation in* $\psi(\eta)$ *with* S

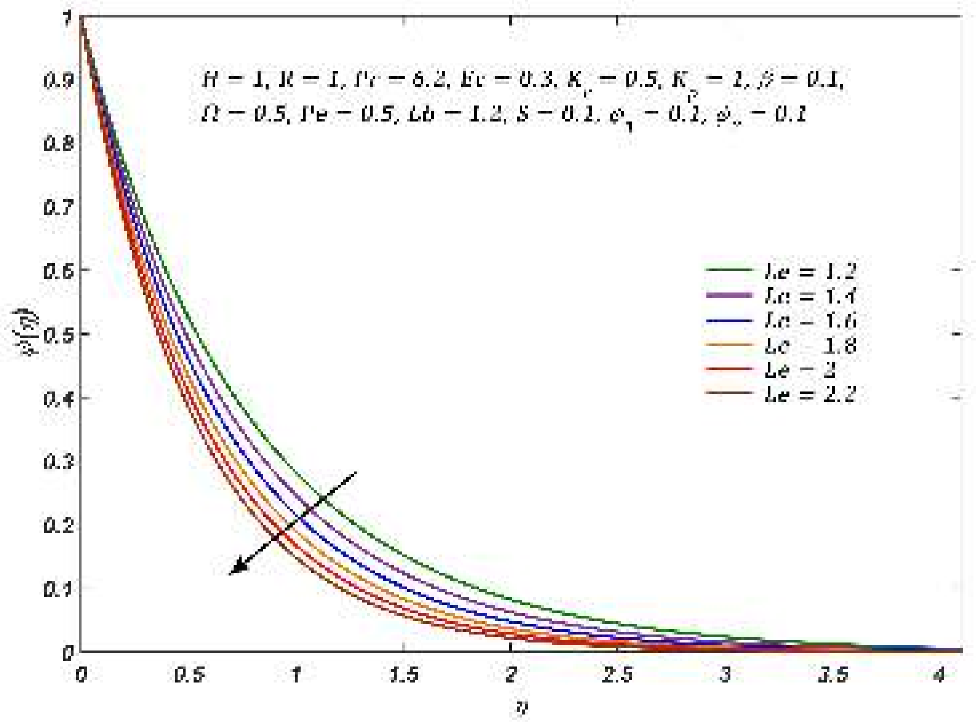

Figure 5.16: *Variation in* $\psi(\eta)$ *with* Le

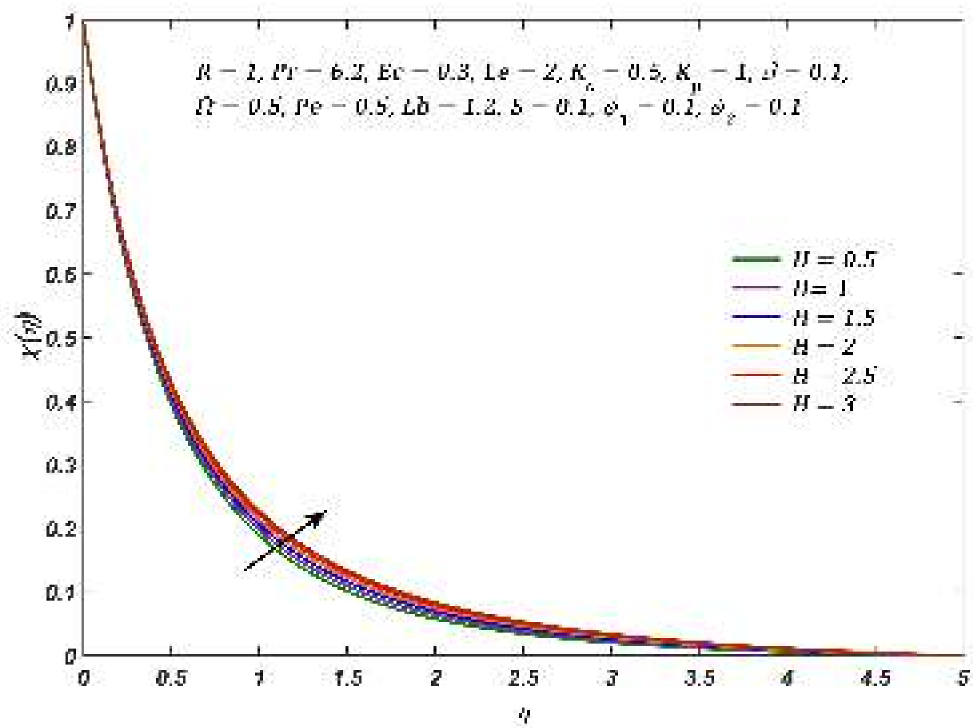

Figure 5.17: *Variation in $\chi(\eta)$ with M*

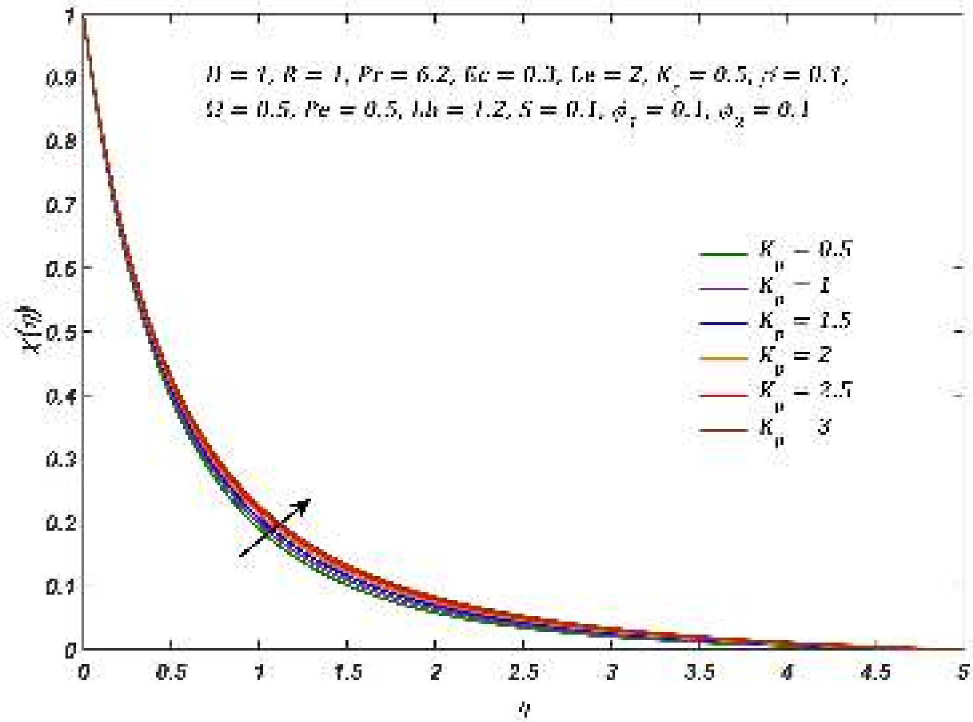

Figure 5.18: *Variation in $\chi(\eta)$ with K_p*

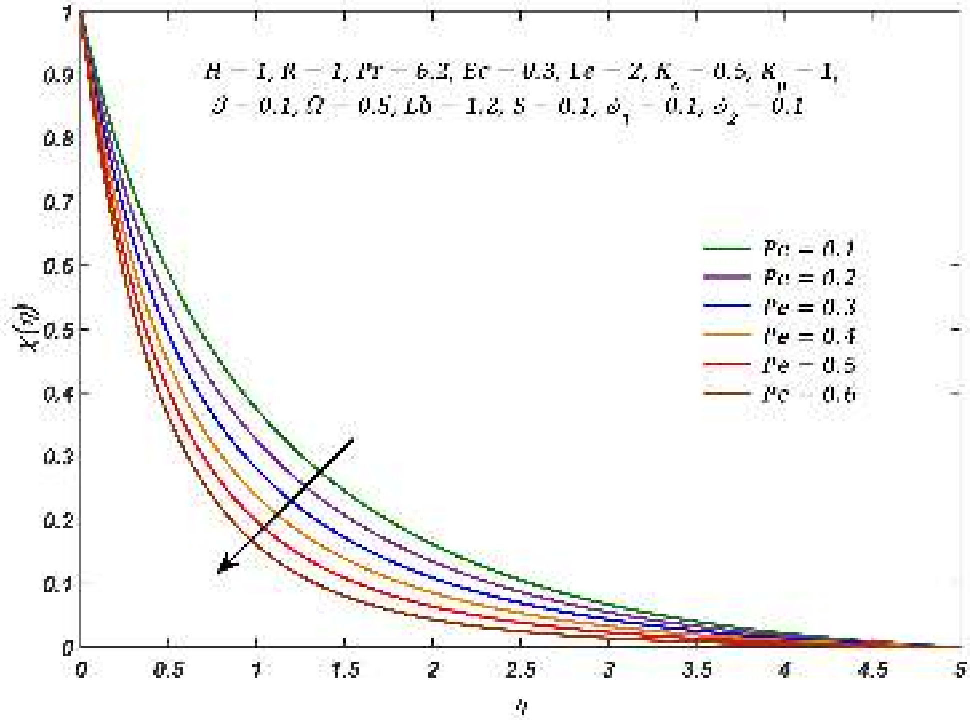

Figure 5.19: *Variation in* $\chi(\eta)$ *with* Pe

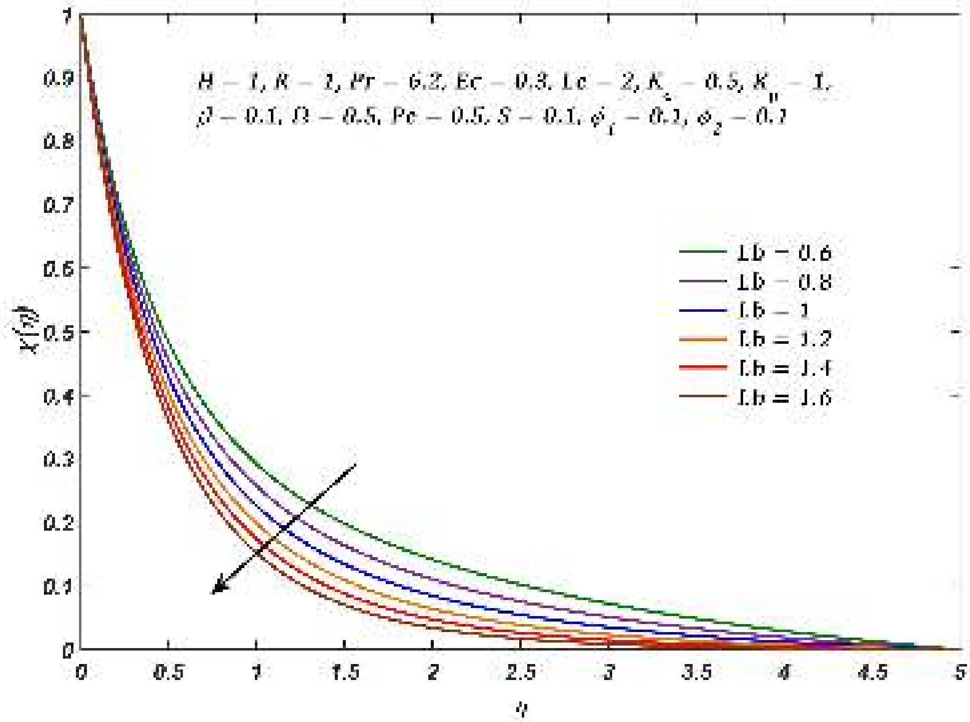

Figure 5.20: *Variation in* $\chi(\eta)$ *with* Lb

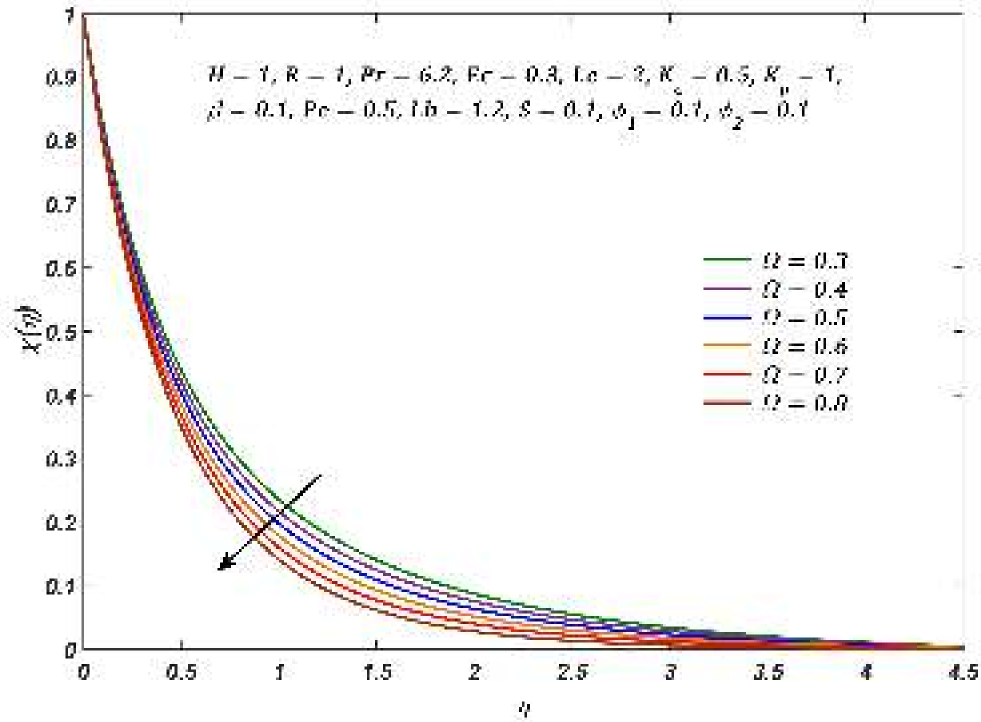

Figure 5.21: *Variation in* $\chi(\eta)$ *with* Ω

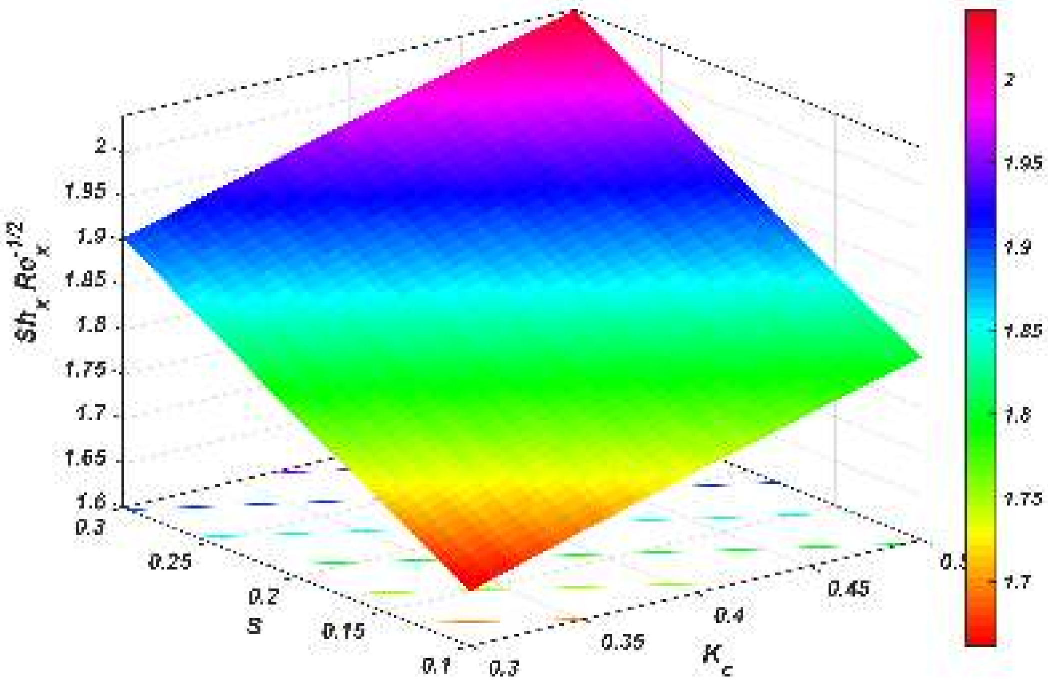

Figure 5.22: *Variation in* $Sh_xRe_x^{-1/2}$ *with* K_c *and* S

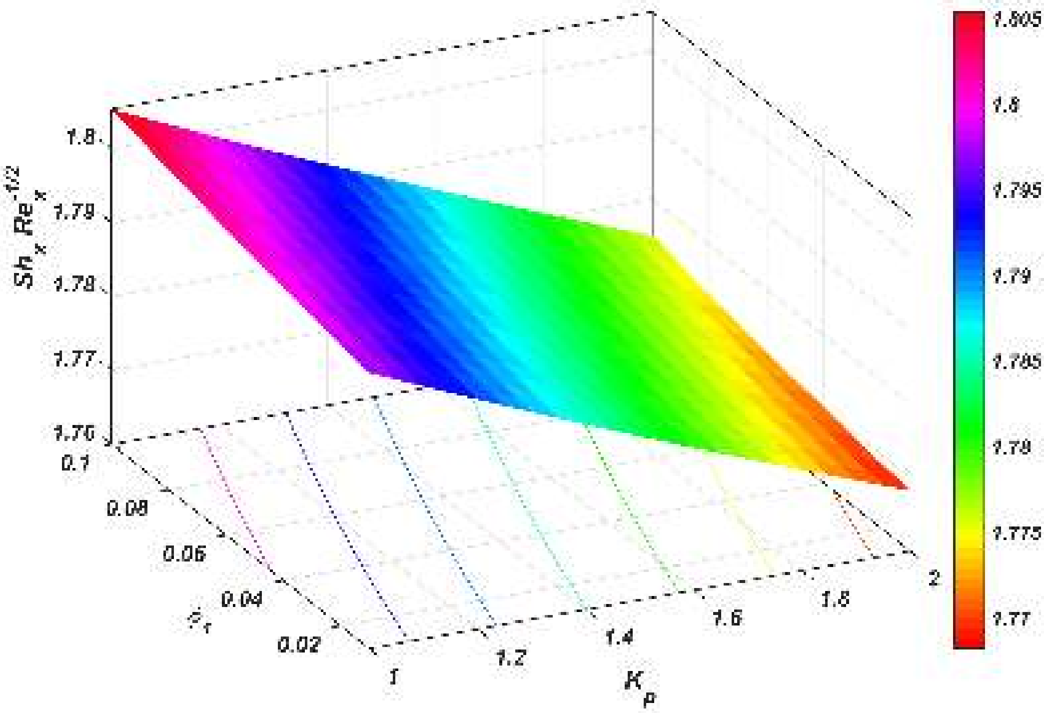

Figure 5.23: *Variation in* $Sh_x Re_x^{-1/2}$ *with* K_p *and* ϕ_1

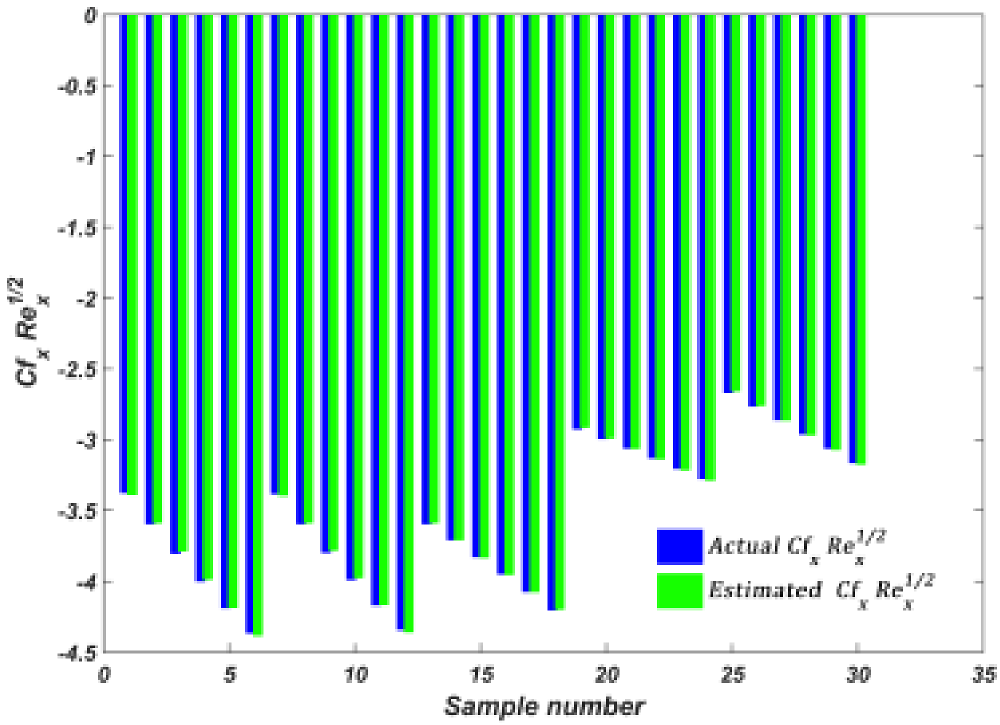

Figure 5.24: *Actual versus estimated* $Cf_x Re_x^{1/2}$

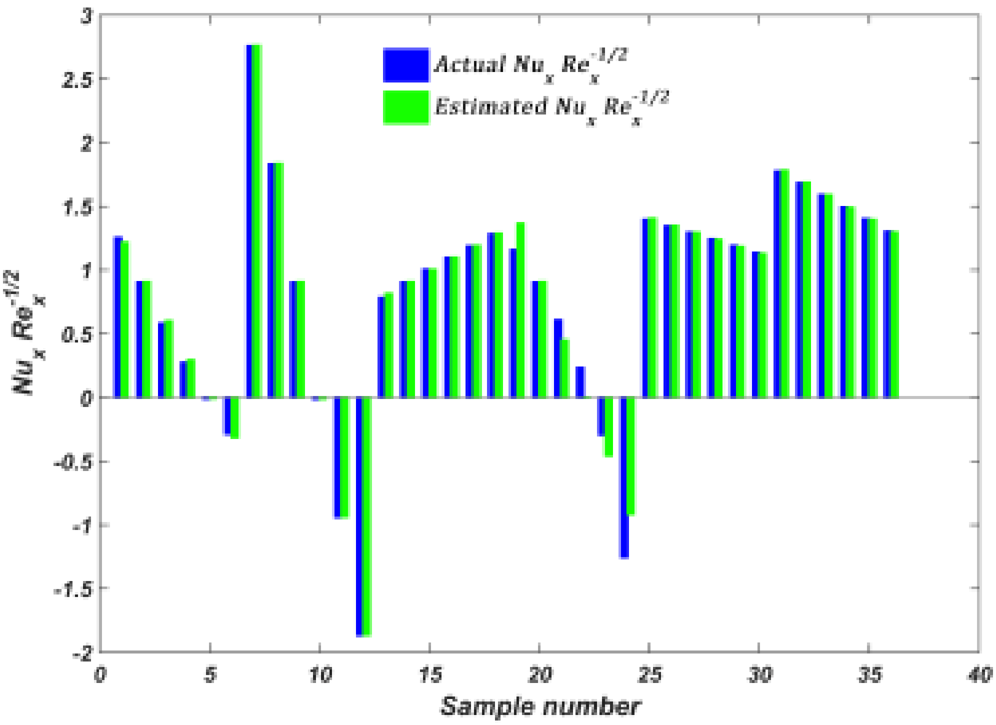

Figure 5.25: *Actual versus estimated* $Nu_x Re_x^{-1/2}$

APPENDIX I: Non-Dimensional Quantities

$H = \frac{2LB_0^2\sigma_f}{c\rho_f}$	Hartmann Number
$Pr = \frac{\mu_f (C_p)_f}{k_f}$	Prandtl Number
$Ec = \frac{u_w^2}{(C_p)_f (T_w - T_\infty)}$	Eckert Number
$R = \frac{4\sigma^* T_\infty^3}{k^* k_f}$	Radiation Parameter
$Le = \frac{\vartheta_f}{D_B}$	LewisNumber
$\Omega = \frac{N_\infty}{N_w - N_\infty}$	Microorganism Concentration Difference Parameter
$Pe = \frac{bW_c}{D_m}$	Bioconvection Peclet Number
$Lb = \frac{\vartheta_f}{D_m}$	Bioconvection Lewis Number
$K_c = \frac{2LK_0}{c}$	Chemical Reaction Parameter
$S = -v_0\sqrt{\frac{2L}{\vartheta_f c}}$	Suction Parameter
$\beta = \frac{2LQ_0}{c(\rho C_p)_f}$	Heat Source Parameter
$K_p = \frac{2L\vartheta_f}{cK_r}$	Porosity Parameter

Appendix II : Nomenclature

u, v	Velocity components	T	Fluid temperature
C	Concentration of nanoparticles	N	Microbial concentration
C_w	Surface concentration of nanoparticles	T_w	Surface temperature
N_w	Surface concentration of Microorganism	b, c	Constants
C_∞	Ambient concentration of nanoparticles	T_∞	Ambient temperature
N_∞	Ambient concentration of Microorganism	T_0	Reference temperature
C_0	Reference concentration of nanoparticles	Re_x	Reynolds number
N_0	Reference concentration of Microorganism	ν	Kinematic viscosity
θ	Dimensionless temperature	L	Reference length
ψ	Dimensionless concentration of nanoparticles	σ	Electrical conductivity
χ	Dimensionless concentration of Microorganism	ρ	Density
K_r	Permeability of the porous medium	μ	Dynamic viscosity
K_0	Chemical reaction coefficient	α	Thermal diffusivity
D_m	Microorganisms diffusion coefficient	q_r	Radiative heat flux
W_c	Maximum cell swimming speed	C_p	Specific heat
v_0	Initial strength of suction	f'	Dimensionless velocity
ϕ_1	Volume fraction of TiO_2	f	Base fluid
ϕ_2	Volume fraction of Ag	nf	Nanofluid
B_0	Magnetic field strength	hnf	Hybrid nanofluid
D_B	Brownian diffusion coefficient	s_1	TiO_2 nanoparticle
Q_0	Heat generation coefficient	s_2	Ag nanoparticle